TWO-DIMENSIONAL SUBSONIC WIND TUNNEL

EVALUATION OF A 20-PERCENT-THICK
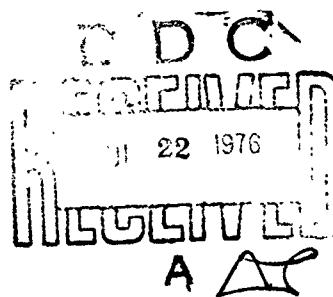
CIRCULATION CONTROL AIRFOIL

Jane Abramson

APPROVED FOR PUBLIC RELEASE: DISTRIBUTION UNLIMITED

ASED 311

June 1975

DAVID
W.
TAYLOR
NAVAL
SHIP
RESEARCH
AND
DEVELOPMENT
CENTER

BETHESDA
MARYLAND
20084

DDC

22 1976

RECEIVED

A

REPORT DOCUMENTATION PAGE		READ INSTRUCTIONS BEFORE COMPLETING FORM
1 REPORT NUMBER DTNSRDC Report ASED-331	2 GOVT ACCESSION NO.	3 RECIPIENT'S CATALOG NUMBER
4 TITLE (and Subtitle) Two-Dimensional Subsonic Wind Tunnel Evaluation of a 20-Percent-Thick Circulation Control Airfoil.		5 TYPE OF REPORT & PERIOD COVERED Final rept.
		6 PERFORMING ORG. REPORT NUMBER
7 AUTHOR(s) Jane Abramson		8 CONTRACT OR GRANT NUMBER(s)
9 PERFORMING ORGANIZATION NAME AND ADDRESS David W. Taylor Naval Ship R&D Center Code 1619 Bethesda, MD 20084		10 PROGRAM ELEMENT, PROJECT, TASK AREA & WORK UNIT NUMBERS
11 CONTROLLING OFFICE NAME AND ADDRESS		12 REPORT DATE June 1975
		13 NUMBER OF PAGES 28
14 MONITORING AGENCY NAME & ADDRESS(if different from Controlling Office)		15 SECURITY CLASS (of this report) Unclassified
		15a DECLASSIFICATION/DOWNGRADING SCHEDULE

16 DISTRIBUTION STATEMENT (of this Report)

Approved for Public Release: Distribution Unlimited

17 DISTRIBUTION STATEMENT (of the abstract entered in Block 20, if different from Report)

18 SUPPLEMENTARY NOTES

19 KEY WORDS (Continue on reverse side if necessary and identify by block number)

Two-Dimensional Wind Tunnel Testing
Circulation Control Airfoils
Elliptic Airfoil Sections
Tangential Blowing
Boundary Layer Control

20 ABSTRACT (Continue on reverse side if necessary and identify by block number)

A circulation control uncambered elliptic airfoil section with a thickness-to-chord ratio of 0.20 was tested subsonically to determine its aerodynamic characteristics. Lift coefficients up to 5 were produced at momentum coefficients of 0.24. The initially high unblown drag coefficients, characteristic of bluff trailing edge airfoils, were greatly reduced at low values of momentum coefficient. It was therefore possible to produce equivalent lift-to-drag ratios in excess of 30 when $C_\ell = 1.0$. The ability

20. Cont'd

to produce high lift coefficients essentially independent of angle of attack is indicated by the results of this investigation.

TABLE OF CONTENTS

LIST OF FIGURES

LIST OF TABLES

ABSTRACT

A circulation control uncambered elliptic airfoil
section with a thickness-to-chord ratio of 0.20 was
tested subsonically to determine its aerodynamic
characteristics. Lift coefficients up to 5 were pro-
duced at momentum coefficients of 0.24. The initially
high unblown drag coefficients, characteristic of
bluff trailing edge airfoils, were greatly reduced at
low values of momentum coefficient. It was therefore
possible to produce equivalent lift-to-drag ratios
in excess of 30 when $C_\ell = 1.0$. The ability to produce
high lift coefficients essentially independent of
angle of attack is indicated by the results of this
investigation.

INTRODUCTION

Tangential blowing over the bluff trailing edge of a 20-percent
uncambered ellipse was investigated experimentally. This configuration
is one of a continuing series of two-dimensional circulation control
airfoil sections [1-5] which employ the Coanda effect to obtain high lift
augmentation by tangentially ejecting a sheet of air near the trailing
edge on the upper surface. Because of the Coanda effect, the jet sheet
remains attached to the rounded trailing edge and provides a mechanism
for boundary layer control. The blowing can be thought of as a movement
of the effective aft stagnation point thereby producing an increase in
circulation. For further discussion of this circulation control concept
and its potential applications, the reader is referred to other studies
in the series. [6-10]

The results of this investigation are being used to ascertain the
effects of camber on the aerodynamic characteristics of a two-dimensional
circulation control airfoil section by comparing the data in this report
to that presented earlier by Williams and Howe.[1] Wind tunnel data were
generated during July 1974.

MODEL AND TEST APPARATUS

The fiberglass model is a modification of one previously tested[4] and is based on an analytical ellipse with an 8-inch major axis (chord) and a 20-percent thickness-to-chord ratio. The rounding of the trailing edge to produce a 0.31-inch radius reduced the chord to 7.908 inches. An upper surface tangential slot consisting of a knife-edged steel blade was placed at the 97-percent chord position. The slot exit was the throat of a converging nozzle whose height was adjustable through the use of pitch screws. An undercut was made on the blade in the vicinity of the slot to ensure that flow would exit tangentially to the model surface (see Figure 1). High pressure internal plenum chambers and flow fences were also incorporated into the model. Tables 1 and 2 give coordinates for the model.

The two-dimensional tests were conducted in the 15 x 20 inch subsonic tunnel with a vented test section and plexiglass walls. The plexiglass permits flow visualization be means of tufts ard oil day-glo pigment solution. The model was pressure tapped as shown in Table 2. Lift and pitching moment coefficients were obtained by numerical integration of pressure tap readings as recorded on a multiple-port scanivalve readout system. These coefficients were corrected by the addition of jet reaction components. Standard solid blockage corrections[11] were applied to the measured freestream dynamic pressure; no wake blockage factor was used because of the uncertain effects of the jet.

Drag measurements were made by using a drag rake placed 1.5 chord lengths downstream of the model inclined at 15 degrees to the freestream. The rake employs 54 total and 8 static pressure tubes, with the heaviest concentration of tubes near the center height. The momentum deficit methods of Betz and Jones[12] were then used to determine the drag coefficient. An addition of $\dot{m}V_\infty/q_\infty S$ was then made to the drag coefficient to account for the additional jet momentum.

Past practice has been to employ separate plenums with high pressure air sources at the junction of the model and tunnel wall to prevent wall boundary layer separation. Although the present model was equipped with such plenums, it was decided after careful analysis of preliminary data

2

that they would not be used because of damage previously sustained by the model. A series of model spanwise taps located near the trailing edge was utilized to record the lateral pressure distribution which was carefully monitored during the test run as an indication of two-dimensionality. The corrections to the resulting data using potential flow will be discussed later in the report.

Mass flow rate ($\dot{m}$) was measured by a calibrated orifice plate inserted in the supply line. To ensure high accuracy for low mass flow data, a second orifice plate with the appropriate calibration range was used for the lower values of C_μ. The jet velocity was calculated by assuming isentropic expansion from duct stagnation pressure to the freestream static pressure as follows:

$$V_j = a_j M_j = (\gamma R T_j)^{\frac{1}{2}} M_j = \left[2RT_t \left(\frac{\gamma}{\gamma-1}\right) \left[1 - \left(\frac{P_\infty}{P_t}\right)^{\frac{\gamma-1}{\gamma}} \right] \right]^{-\frac{1}{2}}$$

The momentum coefficient was then defined as $C_\mu = (\dot{m} V_j / q_\infty S)$. The limiting value of C_μ was determined by consideration of the maximum safe internal plenum pressure for this particular model and/or that pressure which would result in jet impingement on the tunnel floor. Such impingement could cause separation of the floor boundary layer as well as inaccuracies in the drag rake data.

A series of runs was made at freestream dynamic pressures from 10 to 30 psf (Figure 2) corresponding to a model Reynolds number range from 2.4×10^5 to 4.2×10^5. No significant effect of Re on the data was noted and $q_\infty = 20$ psf was chosen to allow for a wider range of C_μ.

RESULTS AND DISCUSSION

The characteristics of the 20-percent uncambered ellipse were evaluated for a single slot height of 0.01 inch (slot height/chord = 0.00126), momentum coefficient C_μ ranging from 0 to 0.26, and angles of attack α ranging from -20 to 8 degrees. Figure 3 depicts the variation of momentum coefficient with duct pressure for the test dynamic pressure of 20 psf.

The expansion of the slot caused by the pressurization of the duct is shown in Figure 4. These data were obtained by pressurizing the duct and measuring the resulting slot height with a thickness gage under quiescent tunnel conditions.

LIFT

Figures 5 and 6 show the sectional lift coefficients determined by integration of the midspan taps. Figure 5, which is an expanded scale plot including closely spaced low momentum coefficient data, revealed the possible existence of a discontinuity in the lift slope. The density of data points taken in previous investigations of circulation control two-dimensional models has been such that detection of a discontinuity in the lift curve slope (dC_ℓ/dC_μ) would be unlikely. However, a change in the slope was reported by Englar[3]. Oil flow studies performed during the evaluation of this model indicated that the flow ahead of the slot was separated under conditions of no blowing ($C_\mu = 0$). This discontinuity may correspond to the level of blowing required for flow attachment to occur at the slot position. Therefore, the existence of such a discontinuity would depend on the chordwise location of the slot in relation to the flow separation point with no blowing; the possible dependency on Reynolds number was not investigated at this time.

An examination of Figure 6 shows that C_ℓ continually increased with increasing C_μ, indicating that "C_μ stall" had not yet been reached, and it appeared that the lift coefficient could have been increased still further with increased blowing.

Another characteristic evident from Figure 6 was a tendency of the lift curve to "lie over" for $C_\mu > 0.08$, resulting in a smaller lift coefficient than anticipated in view of results reported by Englar[1,2]. Additionally a deviation from the expected lift curve was experienced at $\alpha = +8$ and $+5$ degrees. This phenomenon was particularly pronounced at $\alpha = 8$ degrees and has been noted previously[3]; however in this case a return to predicted values was never obtained. This behavior is apparently due to the aft separation experienced on this model.

4

Further insight may be gained by examining Figure 7 which presents the augmentation ratio as a function of momentum coefficient. The augumentation ratio is defined as $\Delta C_\ell / C_\mu$, where C_ℓ is the increase in lift coefficient above the unblown value for a given value of C_μ and incidence. A significant loss of augmentation is apparent at $\alpha = +8$ degrees and to a lesser extent at $\alpha = +5$ degrees; this affirms the deviation from the expected lift curve slope noted previously in Figure 6. In general the augmentation at higher values of momentum coefficient fall off faster than with previous models. It should be noted at this point that data for $\alpha = 20$ degrees were deliberately omitted; the recording of accurate unblown data was not possible and therefore a computation of augmentation ratio could not be made.

With few minor exceptions, an examination of C_p plots revealed no evidence of leading edge separation bubbles although minor, local upper and lower surface trailing edge separations were common. At large negative angles of attack ($\alpha = -20$ degrees), the lower surface was initially completely separated, but reattachment occurred with increased blowing due to the movement of the leading edge stagnation point to the lower surface. As the jet velocity was increased still further, the lower surface again showed areas of separation in the vicinity of the trailing edge.

The variation of lift coefficient with geometric angle of attack is presented in Figure 8. The slopes of the curves were similar for unstalled flow conditions. Agreement between the theoretical lift curve and experimental results was good for conditions of no blowing.

To complete the discussion of the lift characteristics of the 20-percent ellipse, consideration of effects induced by spanwise nonuniformity is required. The suggested use of flow fences and tip jets (see Englar[3] and Englar and Williams[8]) was not possible in this case for reasons previously discussed, and therefore a determination of the effective angle of incidence was made. For the experimental cases selected, potential flow pressure distributions for several incidences and an adjusted C_ℓ were produced. The adjustment to the lift coefficient required that the increment of lift due to the jet suction peak be determined and subtracted from the experimental lift coefficient. Since this increment would not be

5

theoretically predicted, these distributions were then compared to the experimental pressure distribution until the leading edge stagnation point coincided. A resulting experimental-potential flow match is shown in Figure 9. The agreement was good except for the additional jet suction peak and minor lower surface separation (both not predictable with the use of potential flow). The effective angle of incidence for the experimental data is depicted in Figure 10.

The value of the minimum pressure on the airfoil as a function of lift coefficient is presented in Figures 11 and 12. These data are mainly intended for marine applications of circulation control systems, where cavitation is a function of minimum pressure. Figure 12 is the result of the low-blowing, small alpha test series which would be most appropriate for the above-mentioned application.

DRAG

Figures 13 and 14 indicate the variation of a modified drag coefficient with momentum coefficient. These data result from an integration of the wake deficit using the methods of Jones and Betz[12] which were then modified to account for the additional momentum of the jet, thereby becoming $C_d = C_{d_{rake}} - (\dot{m}V_\infty/qS)$. Both figures indicate a high initial drag at all alphas primarily because of the nature of bluff trailing edge airfoils. The highest initial drag was at $\alpha = -20$ degrees; visually monitoring by manometer tubes indicated that the wake was extending over the entire rake before a no-blowing condition could be reached, and this was attributed to extensive separation on the lower surface. The secondary rise in the drag curve at both $\alpha = -15$ and -20 degrees at $C_\mu \leq 0.2$ was again the result of lower aft separation after reattachment had occurred.

The initial variation of drag with trailing edge blowing can be more easily observed in Figure 13. An initial decrease in drag was immediately noted whenever $\alpha \leq 0$ an initially flat drag distribution was evident for $\alpha = +8$ or $+5$ degrees. This was also evident to a lesser extent at $\alpha = +3$ degrees where the initial decrease in drag was less than at any nonpositive alpha. For $\alpha = 8$ and 5 degrees, this region was found to correspond to

6

the deficit in the lift curve slope previously discussed. Significant thrust recovery was noted in Figure 14 for most alphas, as evidenced by the decreasing drag coefficients.

PITCHING MOMENT

Figure 15 depicts pitching moment about the midchord ($C_{m_{50}}$). As was the case with previous circulation control sections, a negative pitching moment was produced by the relatively high trailing edge suction peaks. The only notable exceptions were at $\alpha = -15$ and -20 degrees for $C_\mu \geq 0.134$. In both those cases, there were large regions of separation on the lower surface of the trailing edge. The resulting region of low pressure reduced the negative pitching moment somewhat.

EQUIVALENT LIFT-DRAG RATIO

Comparison of data taken with and without blowing can best be made when account is taken of the energy expended to produce blowing. Figure 16 presents the lift-to-equivalent-drag ratio as a function of lift coefficient; the equivalent drag is defined here as:

$$d_e = d + \frac{\dot{m}V_j^2}{2V_\infty} + \dot{m}V_\infty$$

The first term d is the momentum deficit as measured by the drag rake (corrected for jet efflux), the second term is the kinetic energy flux, and the third is an intake momentum flux. Thus in coefficient form:

$$\frac{\ell}{d_e} = \frac{C_\ell}{C_d + C_\mu \frac{V_j}{2V_\infty} + C_\mu \frac{V_\infty}{V_j}}$$

A more comprehensive derivation of the above may be found in Englar[3].

The highest value for ℓ/d_e occurred at very low blowing and the maximum value was approximately 40, despite the relatively high lift coefficients. Since the measured value of drag was low throughout a great portion of the experimental test range, the results show the importance of "blowing power" ($C_\mu V_j/2V_\infty$) in the expression for equivalent drag. Thus to obtain high

7

values for ℓ/d_e it becomes necessary to produce high lift coefficients at relatively low values of the blowing coefficients.

CONCLUSIONS

The 20-percent thick circulation control ellipse was evaluated in a subsonic wind tunnel to provide continuing information on a new family of airfoils. The following conclusions were drawn from an examination of the subsonic data:

1. Despite the fact that augmentation ratios were generally lower than obtained in previous test of circulation control airfoils, section lift coefficients of 5.0 were generated for $C_\mu = 0.24$ at an angle of attack of 3 degrees. A lift coefficient of 2 was generated by the section at $\alpha = -20$ degrees.

2. Augmentation ratios in excess of 75 (see Figure 7) were produced at low blowing rates for negative angles of incidence.

3. At $C_\ell = 1.0$, lift-to-equivalent-drag ratios of over 30 were generated.

4. In most cases initiation of blowing reduced the high unblown drag coefficient. In those cases where the value of the drag coefficient remained unchanged until a substantial level of blowing was reached, a low initial lift slope (dC_ℓ/dC_μ) was also indicated.

5. The presence of a possible discontinuity in the lift curve slope (dC_ℓ/dC_μ) may correspond to the movement of the separation point to a position aft of the slot location.

REFERENCES

1. Williams, R. M. and H. J. Howe, "Two-Dimensional Subsonic Wind Tunnel Tests on a 20-Percent Thick, 5-Percent Cambered Circulation Control Airfoil," NSRDC Technical Note AL-176 (AD 877-764) (Aug 1970).

2. Englar, R. J., "Two-Dimensional Subsonic Wind Tunnel Tests of Two 15-Percent Thick Circulation Control Airfoils," NSRDC Technical Note AL-211 (Aug 1971).

3. Englar, R. J., "Two-Dimensional Subsonic Wind Tunnel Tests of a Cambered 30-Percent Thick Circulation Control Airfoil," NSRDC Technical Note AL-201 (May 1972).

4. Williams, R. M., "Some Research on Rotor Circulation Control," Proceedings, Third CAL/AVLABS Symposium, Aerodynamics of Rotary Wing and V/STOL Aircraft, Vol. 2, Buffalo, New York (Jun 1969).

5. Englar, R. J., "Two-Dimensional Transonic Wind Tunnel Tests of Three 15-Percent Thick Circulation Control Airfoils," NSRDC Technical Note AL-182 (Dec 1970).

6. Williams, R. M. and E. O. Rogers, "Design Considerations of Circulation Control Rotors," 28th Annual National Forum of the American Helicopter Society, Washington, D.C. (May 1972; (Available as Preprint 603).

7. Englar, R. J. and R. M. Williams, "Design of a Circulation Control Stern Plane for Submarine Applications," NSRDC Technical Note AL-200 (Mar 1971).

8. Englar, R. J. and R. M. Williams, "Test Techniques for High Lift Two-Dimensional Airfoils with Boundary Layer and Circulation Control for Application to Rotary Wing Aircraft," Canadian Aeronautics and Space Journal, Vol. 19, No. 3 (Mar 1973).

9. Englar, R. J., "Subsonic Wind Tunnel Investigation of the High Lift Capability of a Circulation Control Wing on a 1/5-Scale T-2C Aircraft Model," NSRDC Technical Note AL-299 (May 1973).

10. Wilkerson, J. B., "Design and Performance Analysis of Prototype
    Circulation Control Helicopter Rotor," NSRDC Technical Note AL-290
    (Mar 1973).

11. Pope, Alan, "Wing-Tunnel Testing," Second Edition, John Wiley & Sons,
    Inc., New York, (1964), pp. 307-311.

12. Schlichting, Hermann, "Boundary Layer Theory," Sixth Edition, McGraw-
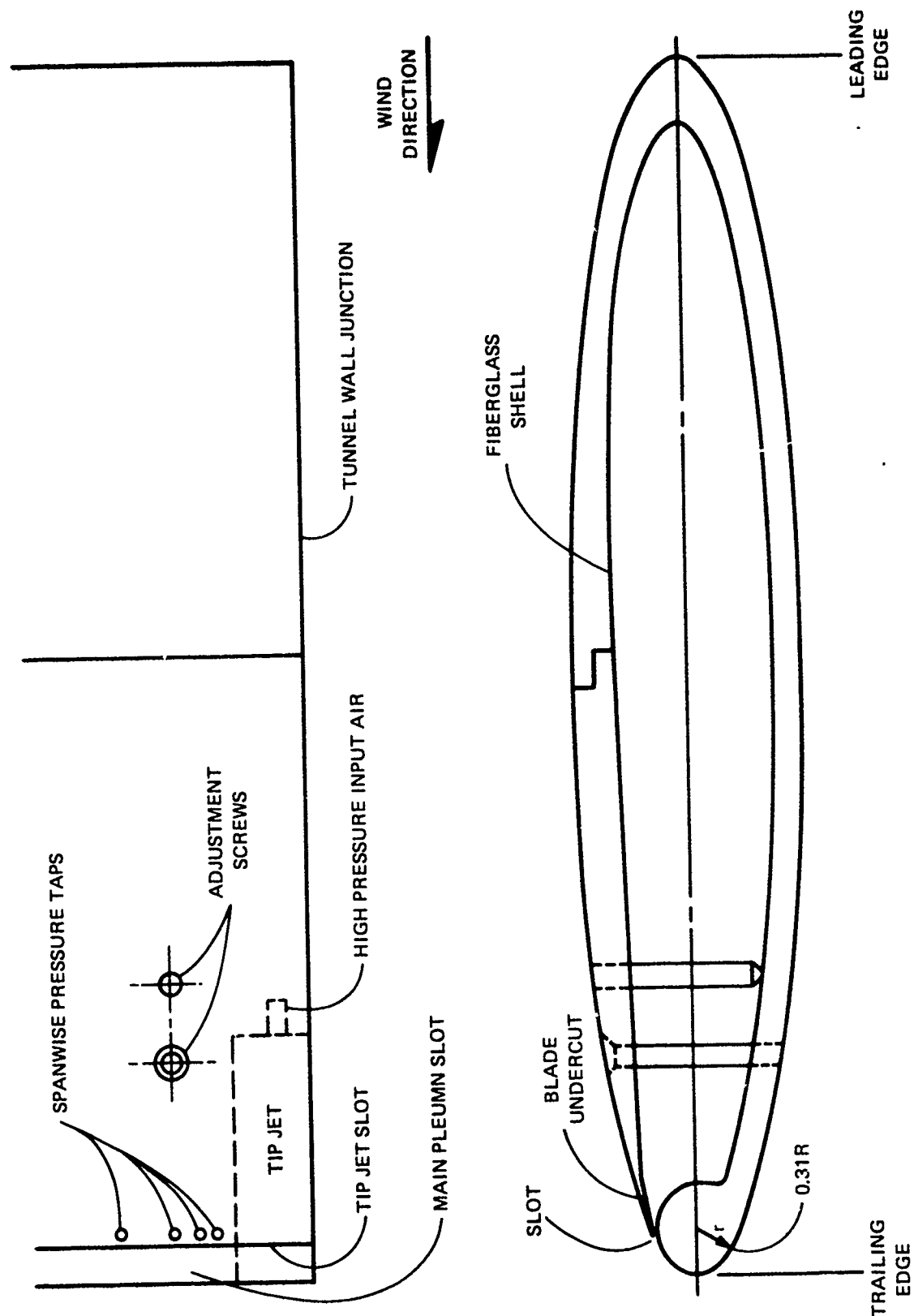   Hill Book Company, New York (1968), pp. 708-713.

SPANWISE PRESSURE TAPS

ADJUSTMENT SCREWS

TIP JET

HIGH PRESSURE INPUT AIR

TIP JET SLOT

MAIN PLEUMN SLOT

TUNNEL WALL JUNCTION

WIND DIRECTION

FIBERGLASS SHELL

LEADING EDGE

BLADE UNDERCUT

SLOT

0.31R

r

TRAILING EDGE

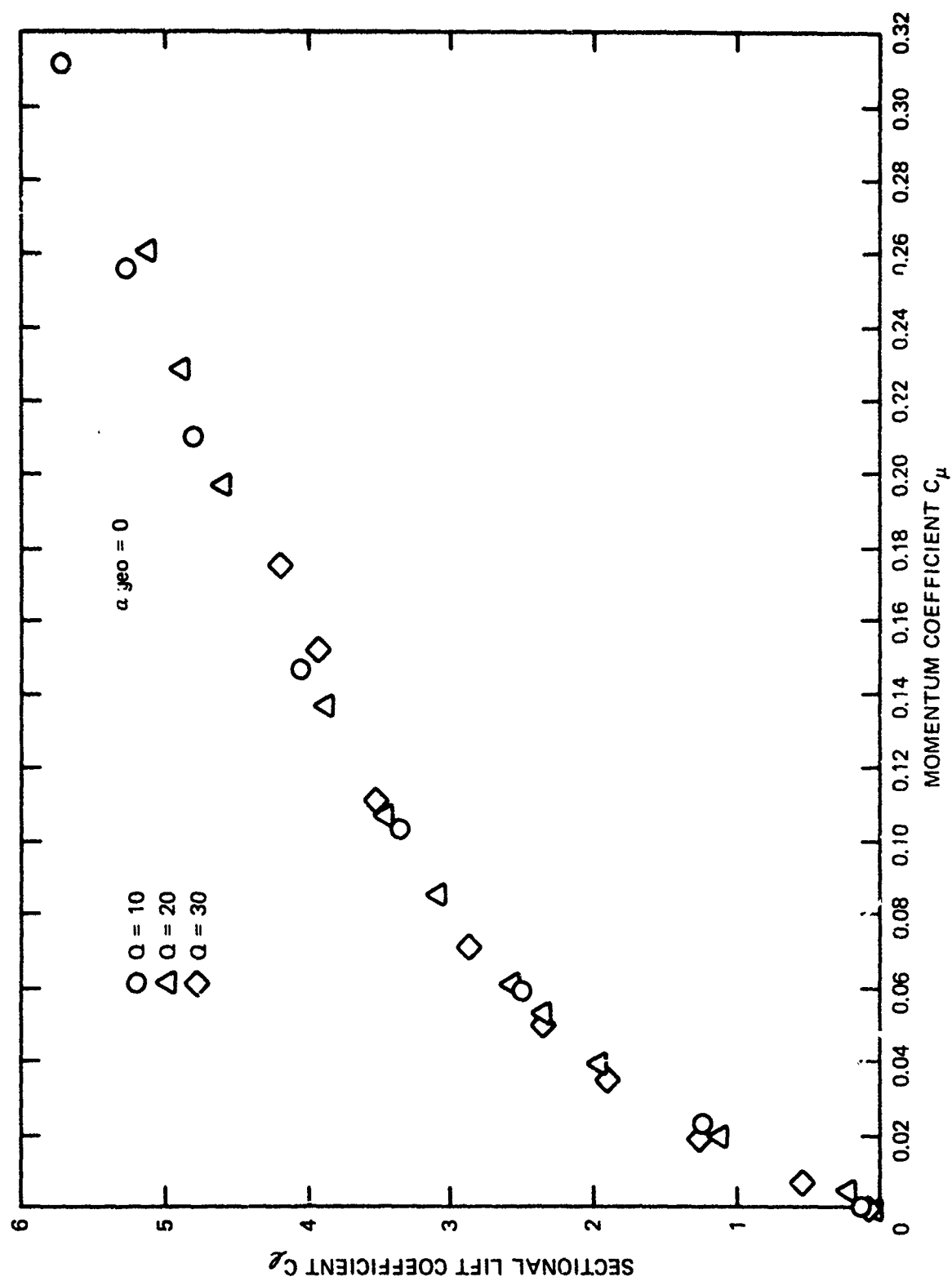Figure 1 – Subsonic Two-Dimensional Model Geometry

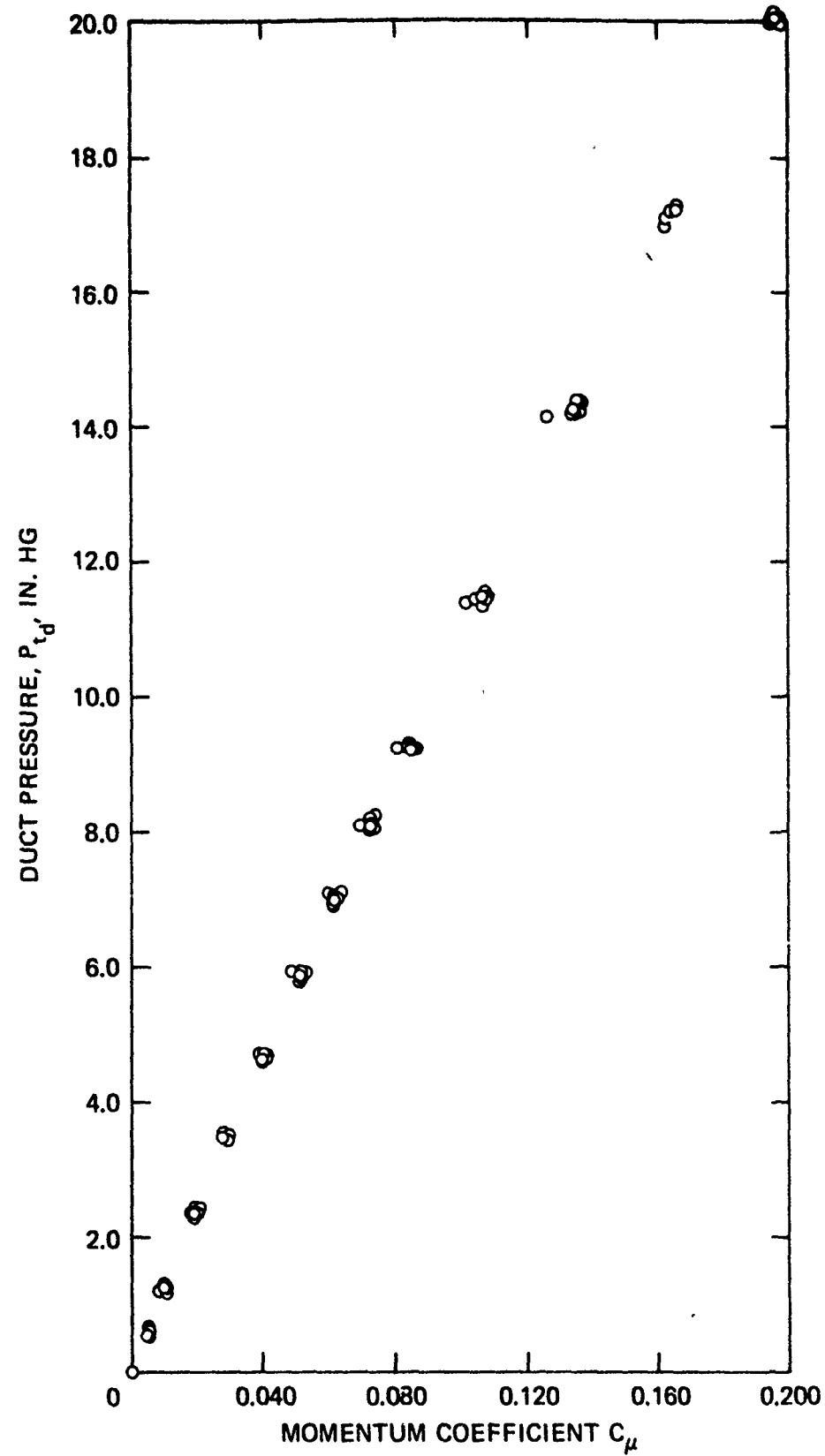11

Figure 2 — Lift Variation with Dynamic Pressure

12

Figure 3 — Experimention Variation of Momentum
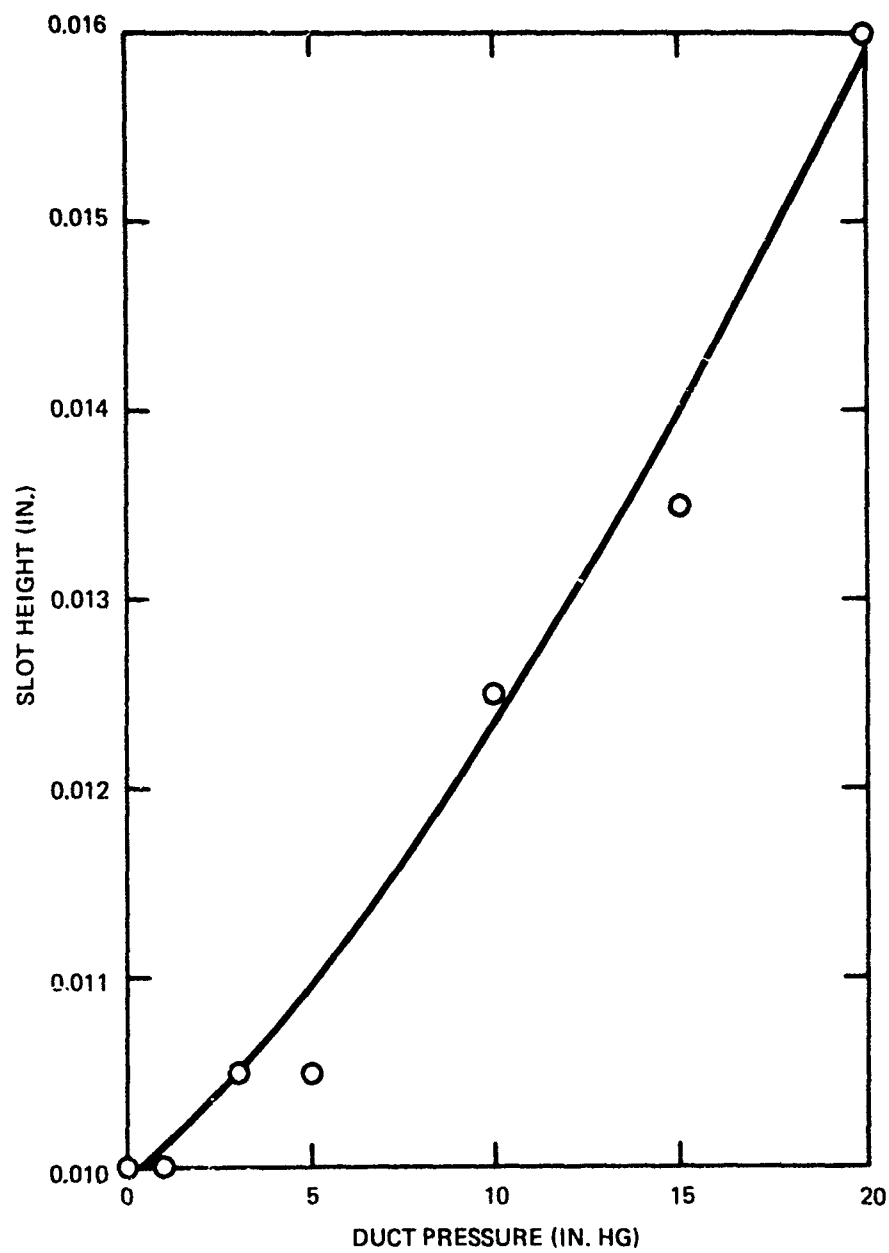Coefficient with Duct Pressure

13

Figure 4 -- Variation of Slot Height with Duct Pressure
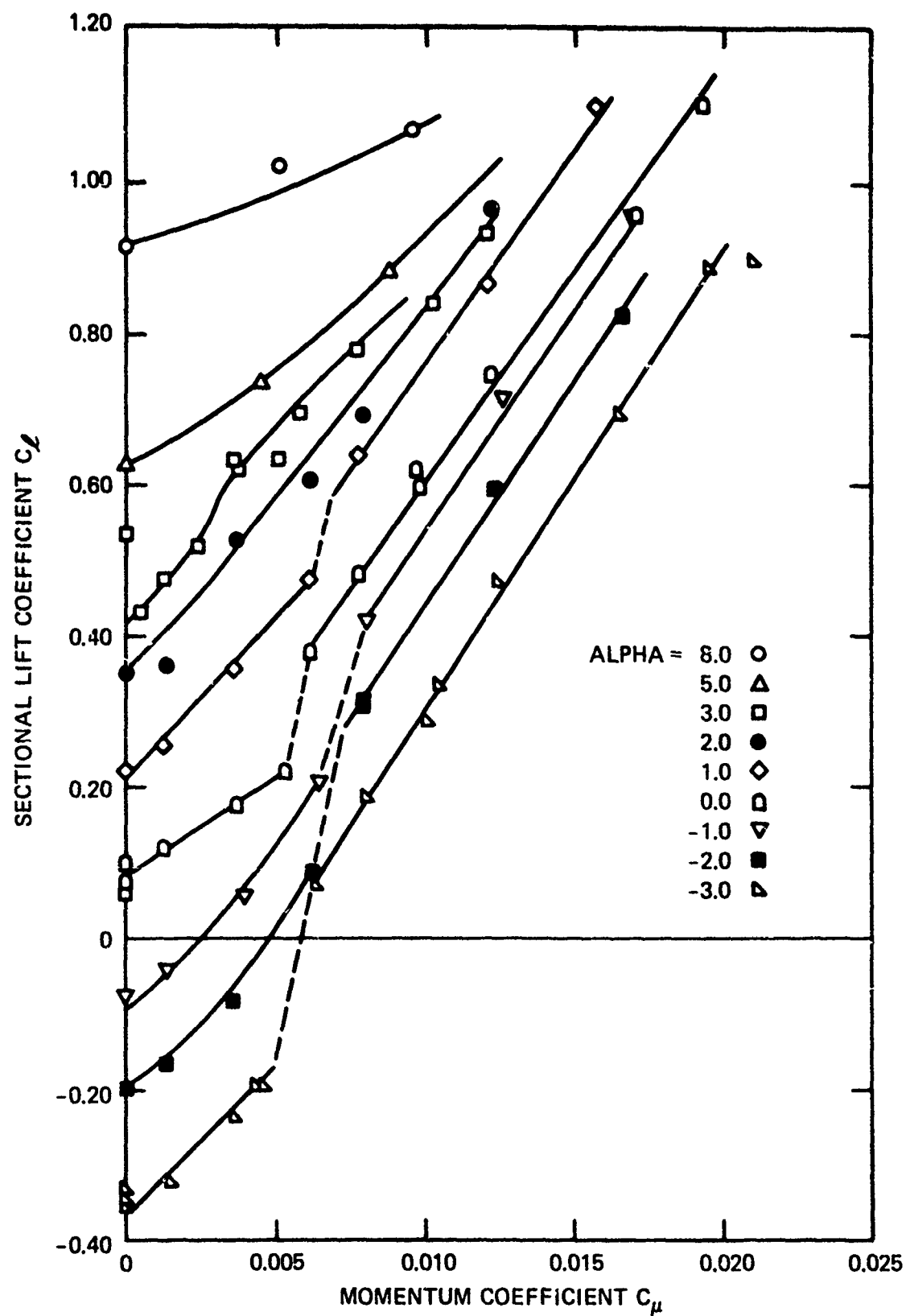
Figure 5 – Lift Variation with Momentum Coefficient
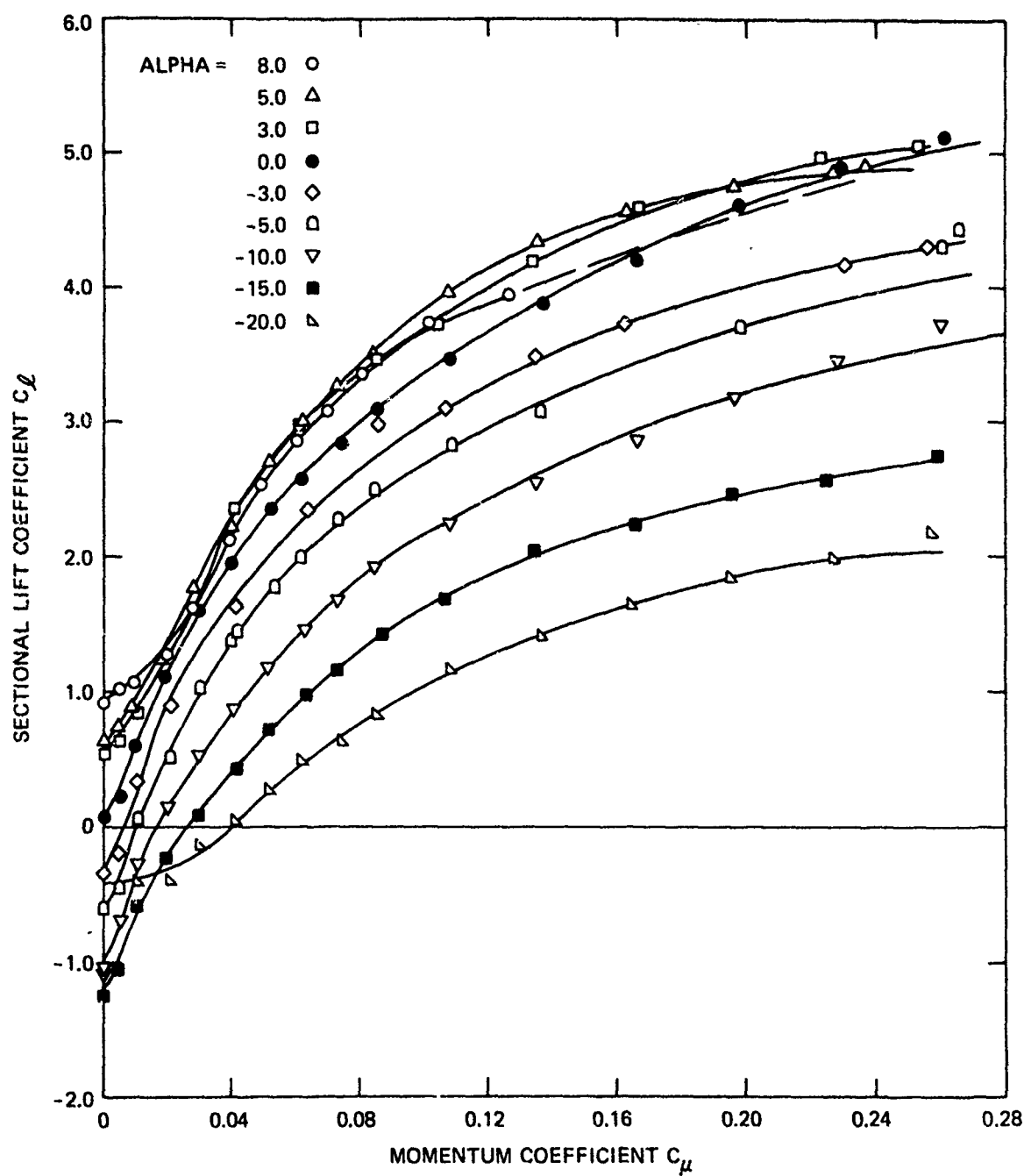(Expanded Scale)

15

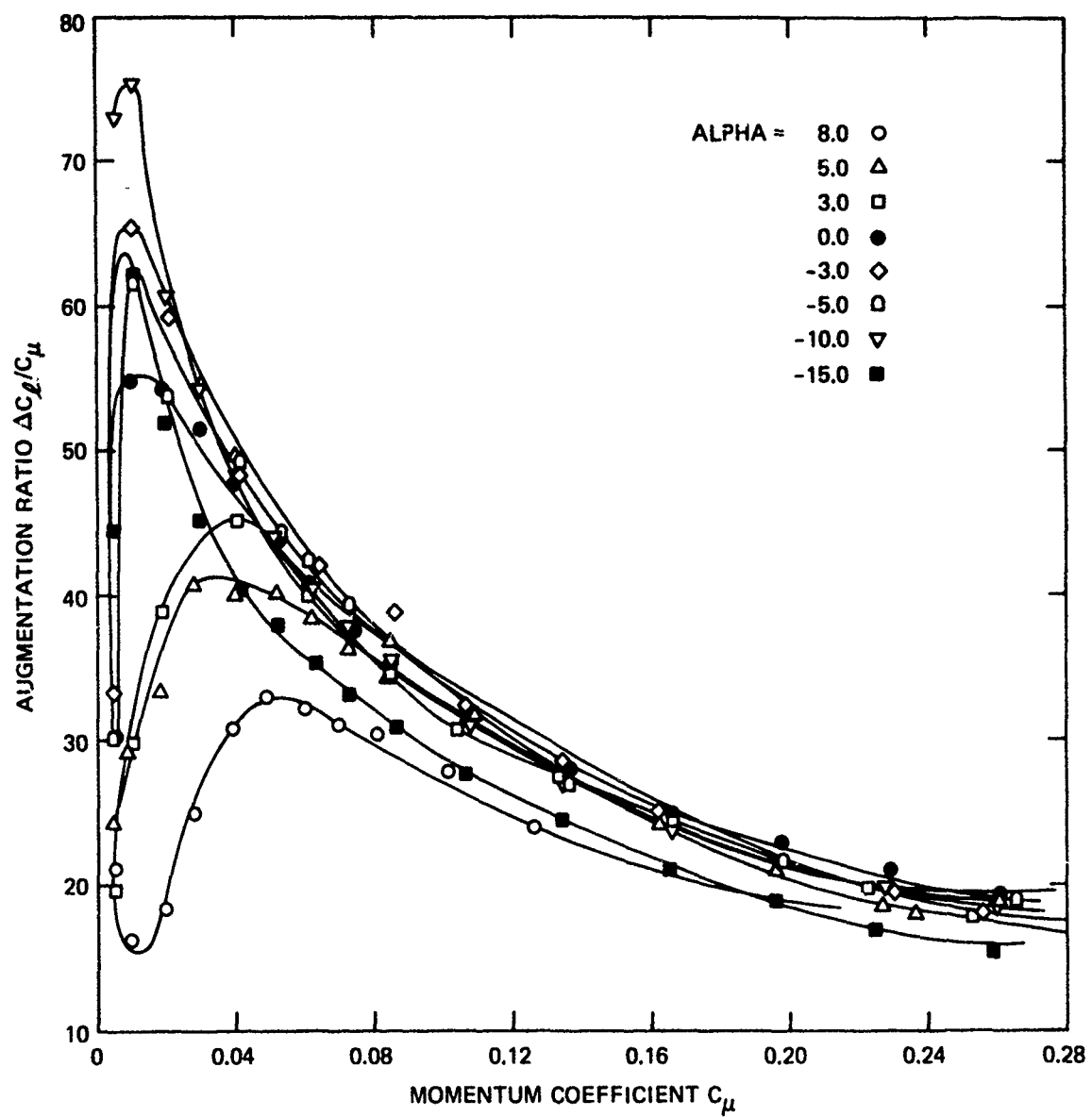Figure 6 — Lift Variation with Momentum Coefficient
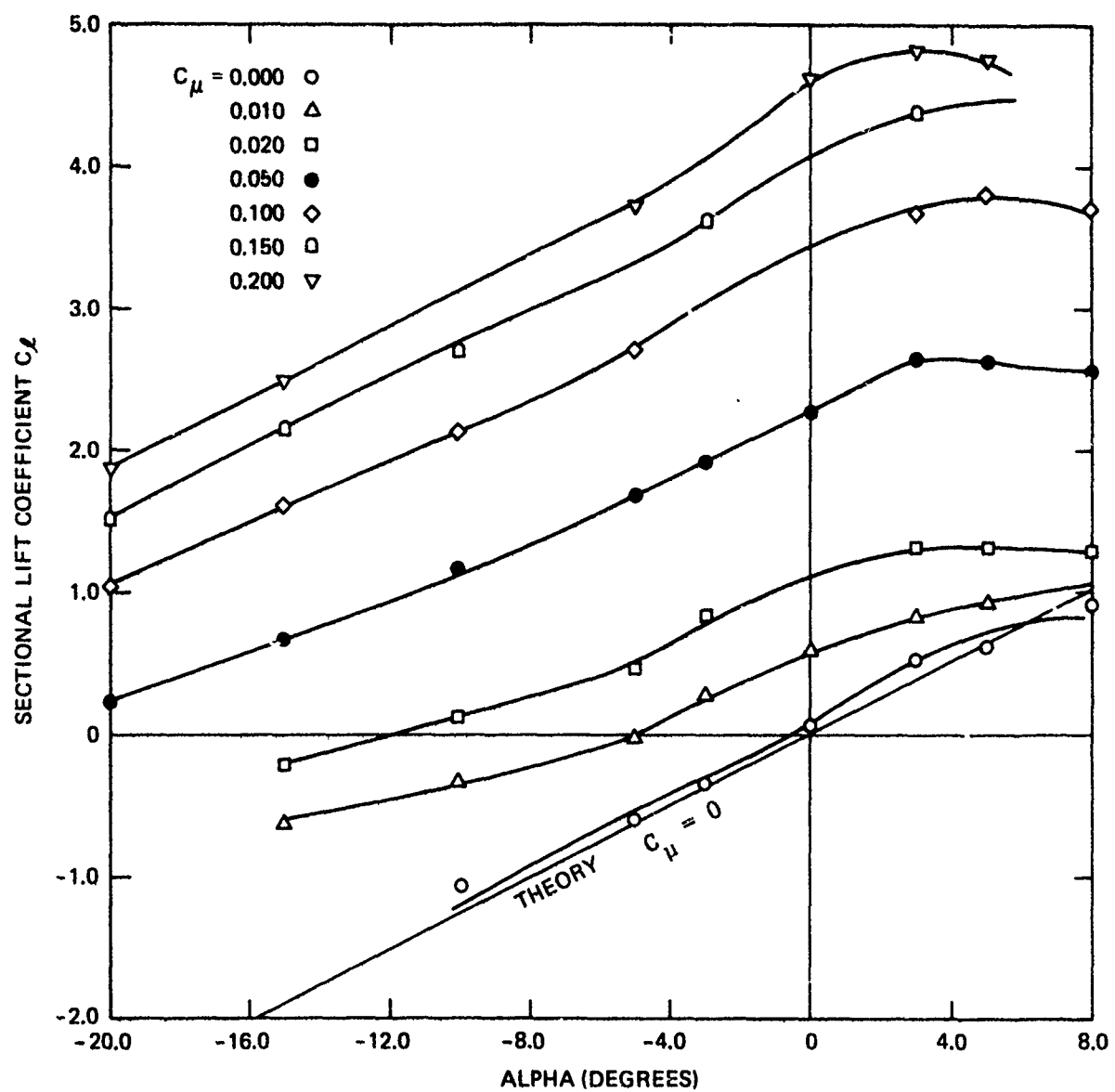
Figure 7 — Lift Augmentation

17

Figure 8 — Lift Variation with Geometric Angle of Attack
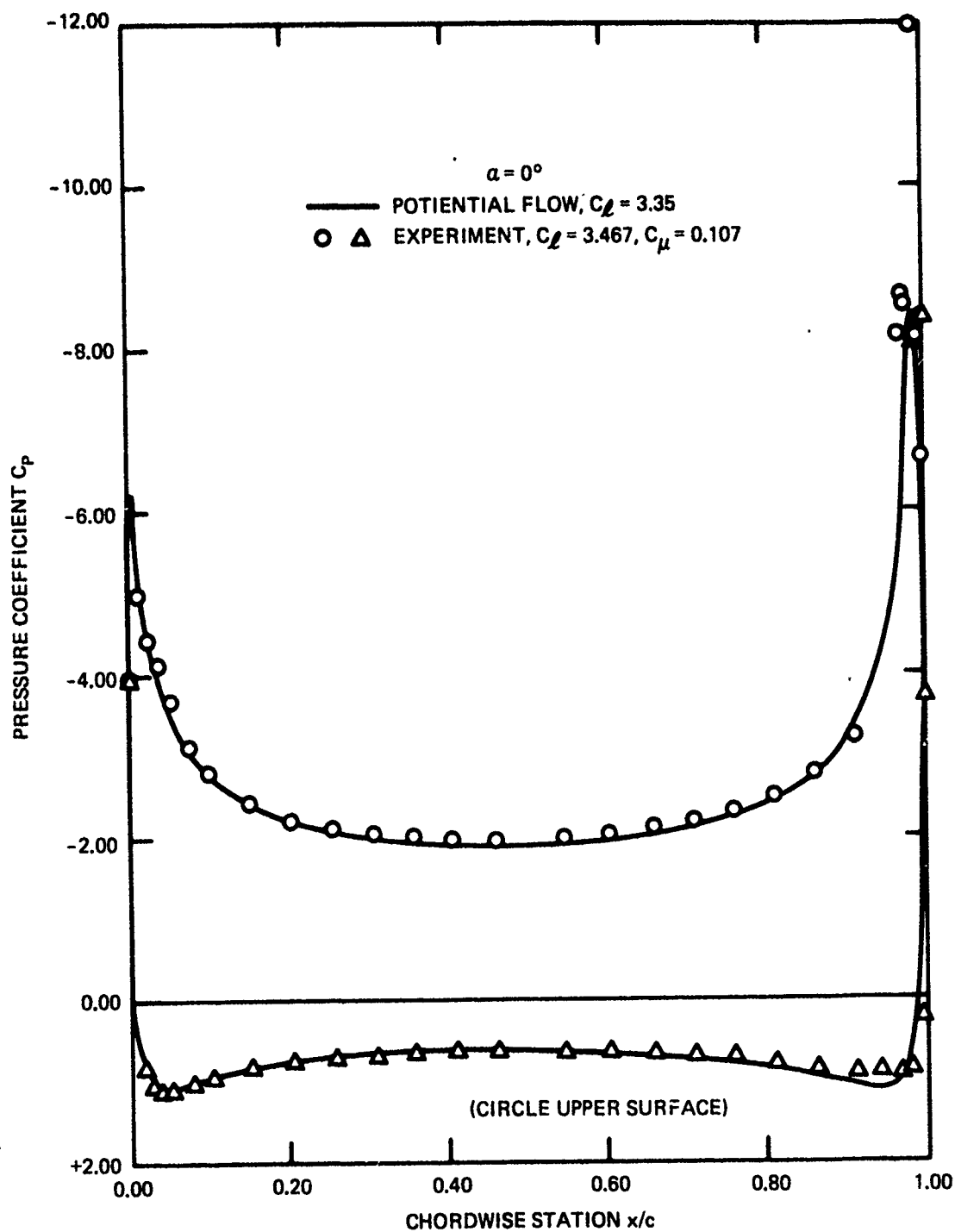
Figure 9 – Comparison of Potential Flow and
Experimental Pressure Distribution
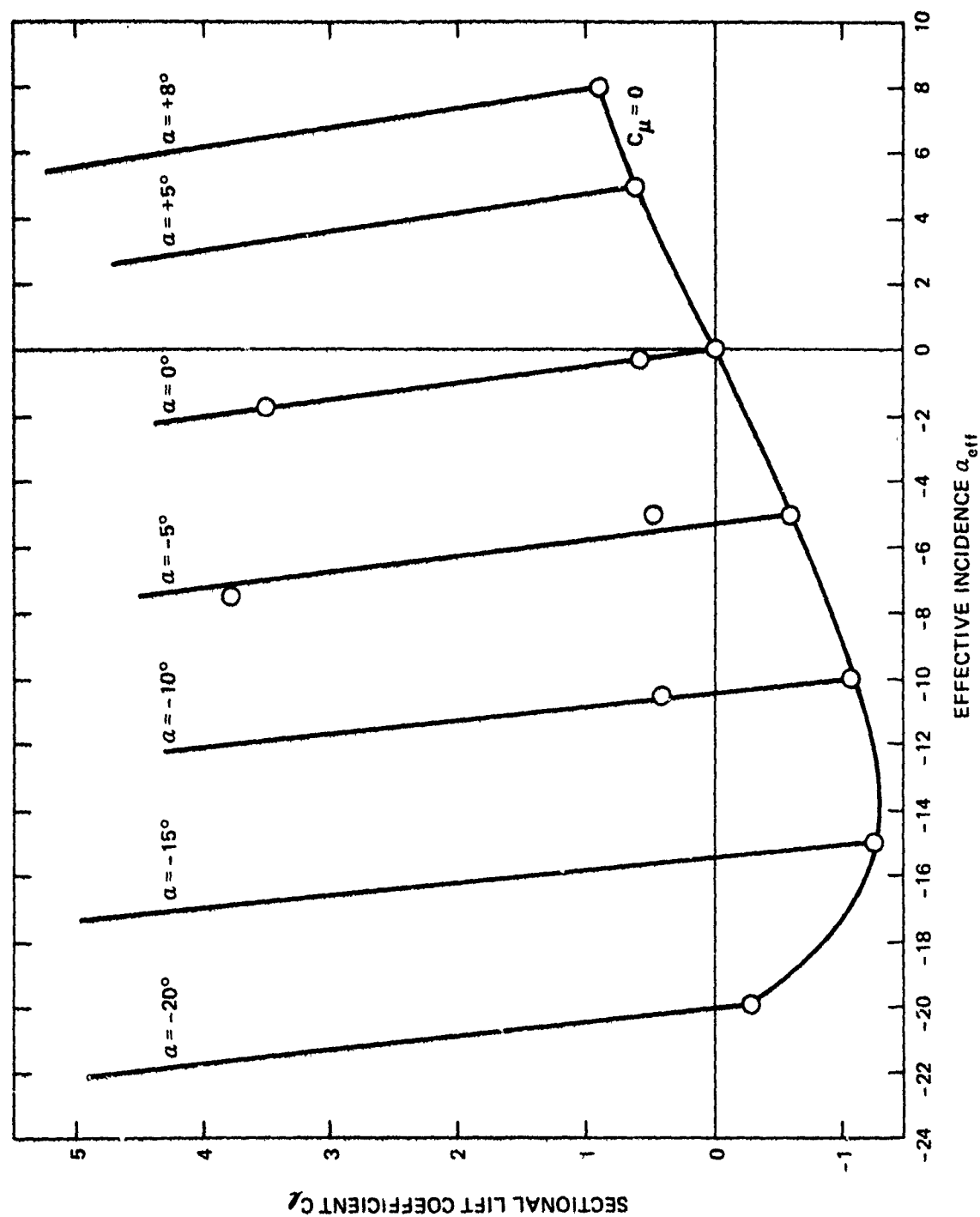
Figure 10 — Induced Angle Corrections to Geometric Incidence

20

MINIMUM PRESSURE COEFFICIENT
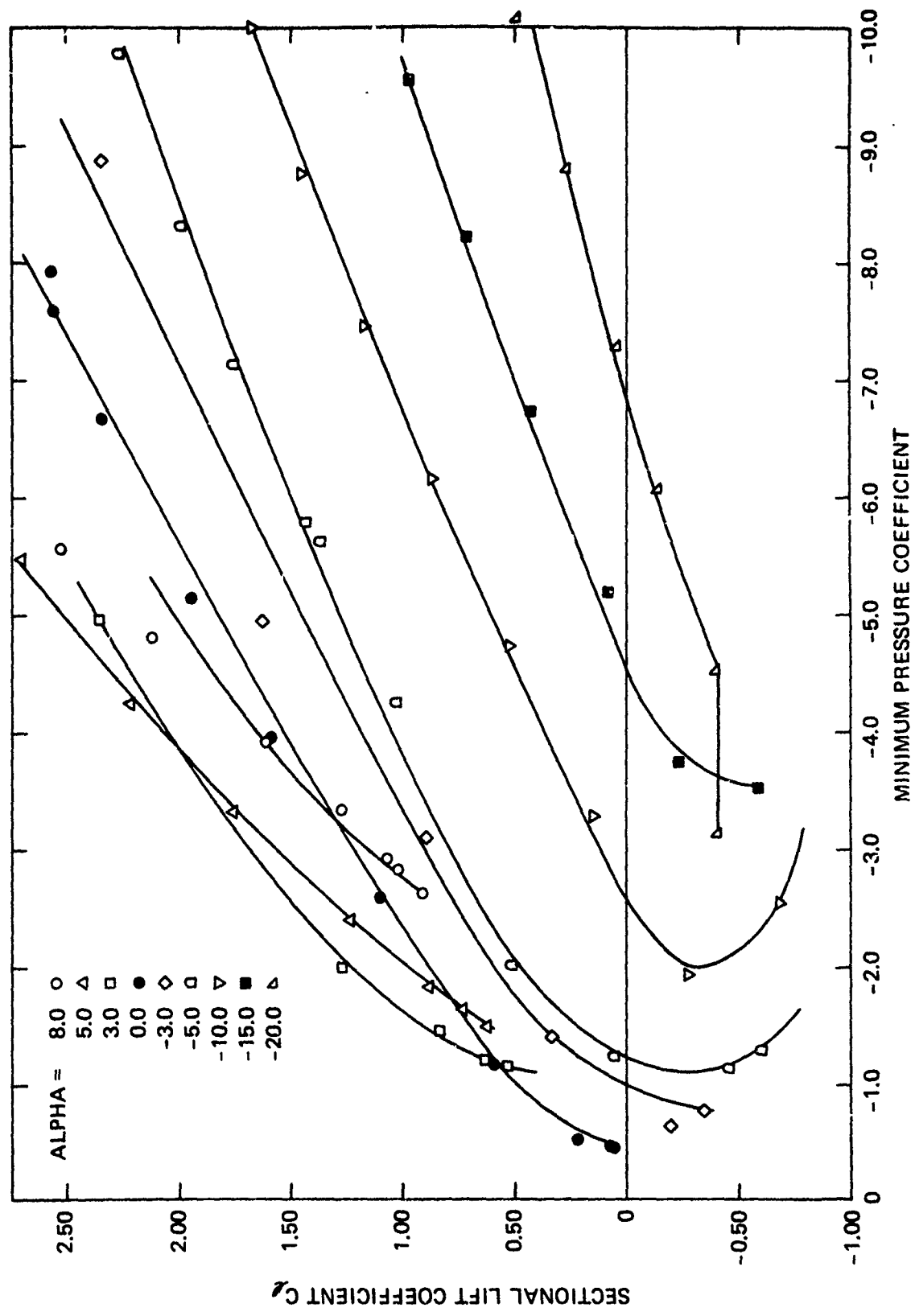
Figure 11 — Minimum Pressure Coefficient

SECTIONAL LIFT COEFFICIENT C_l

ALPHA =

8.0	○
5.0	△
3.0	□
0.0	●
-3.0	◇
-5.0	◻
-10.0	▽
-15.0	■
-20.0	◁

Figure 12 — Minimum Pressure Coefficient for Low
Momentum Coefficients

Figure 13 – Drag Coefficient Variation with Momentum
Coefficient (Expanded Scale)

23

Figure 14 — Drag Coefficient Variation with Momentum Coefficient

Figure 15 — Variation in Half-Chord Pitching Moment Coefficient
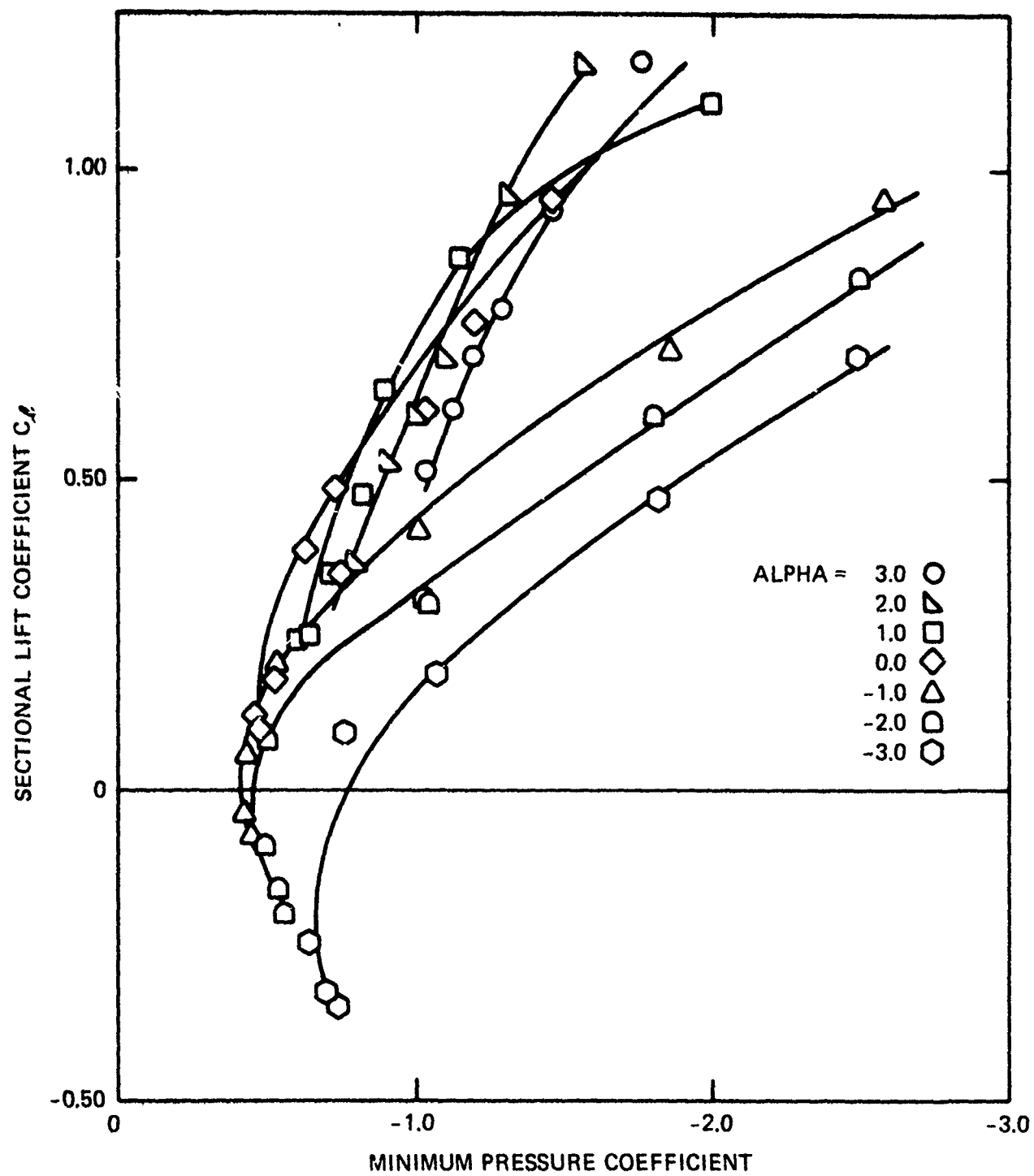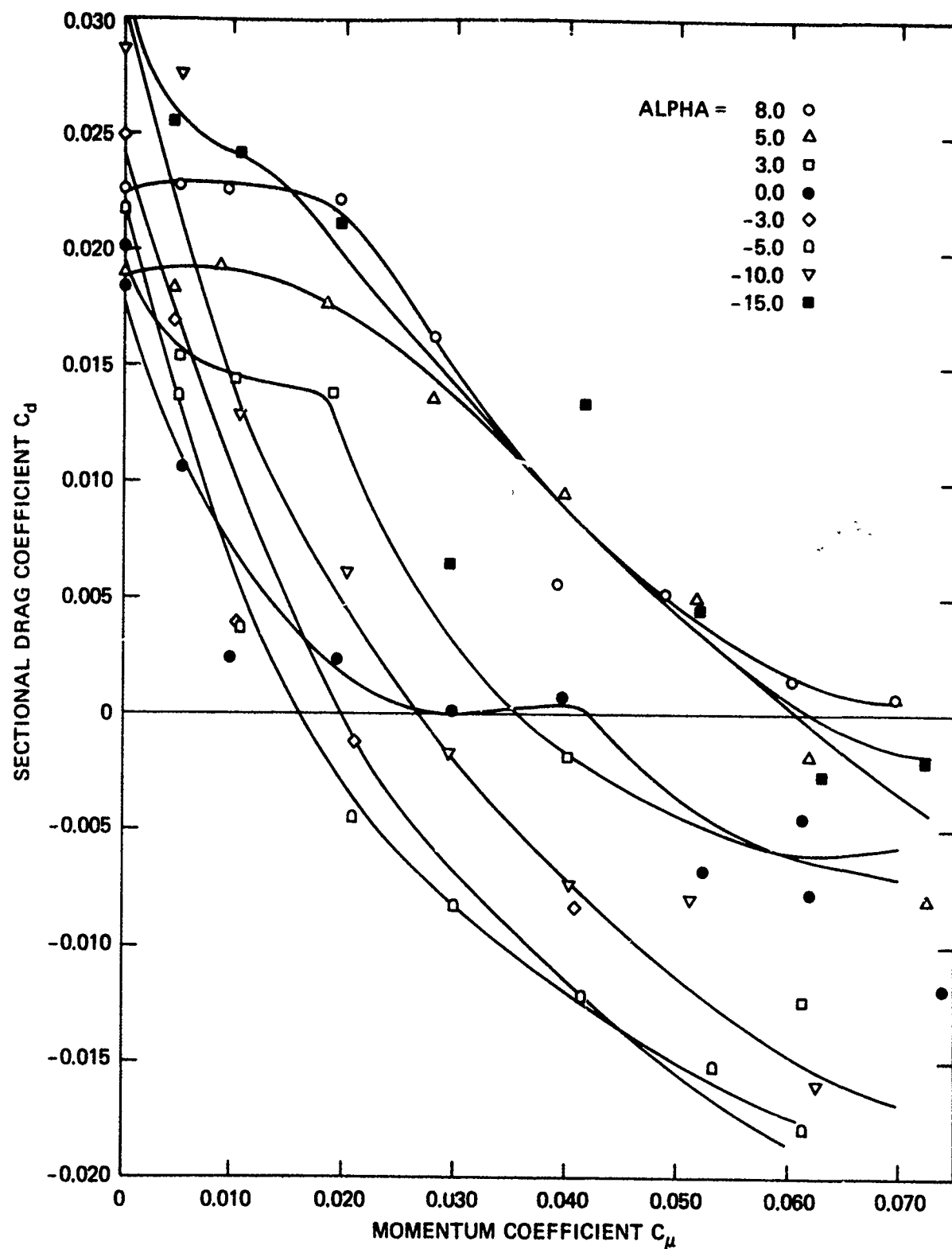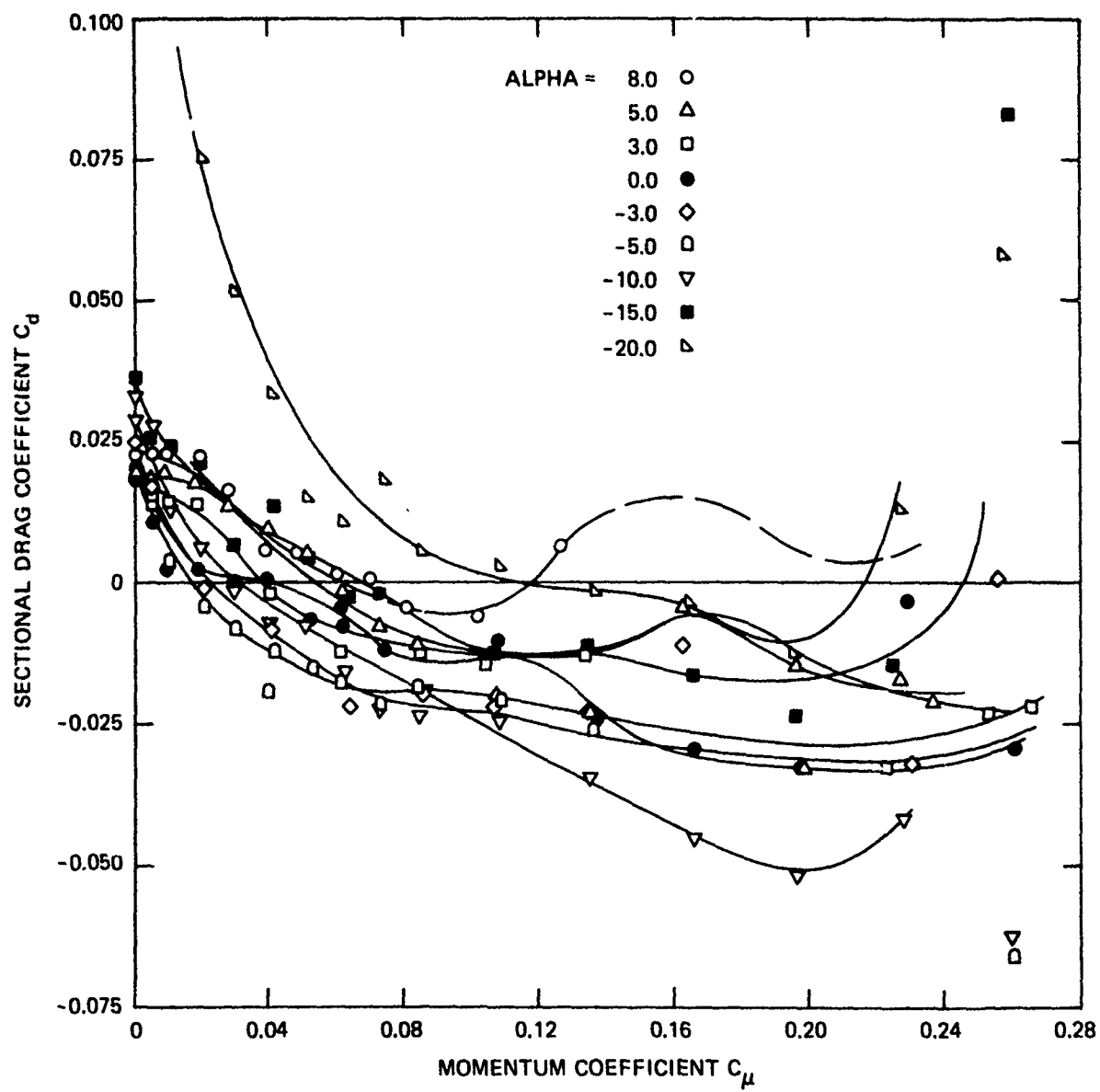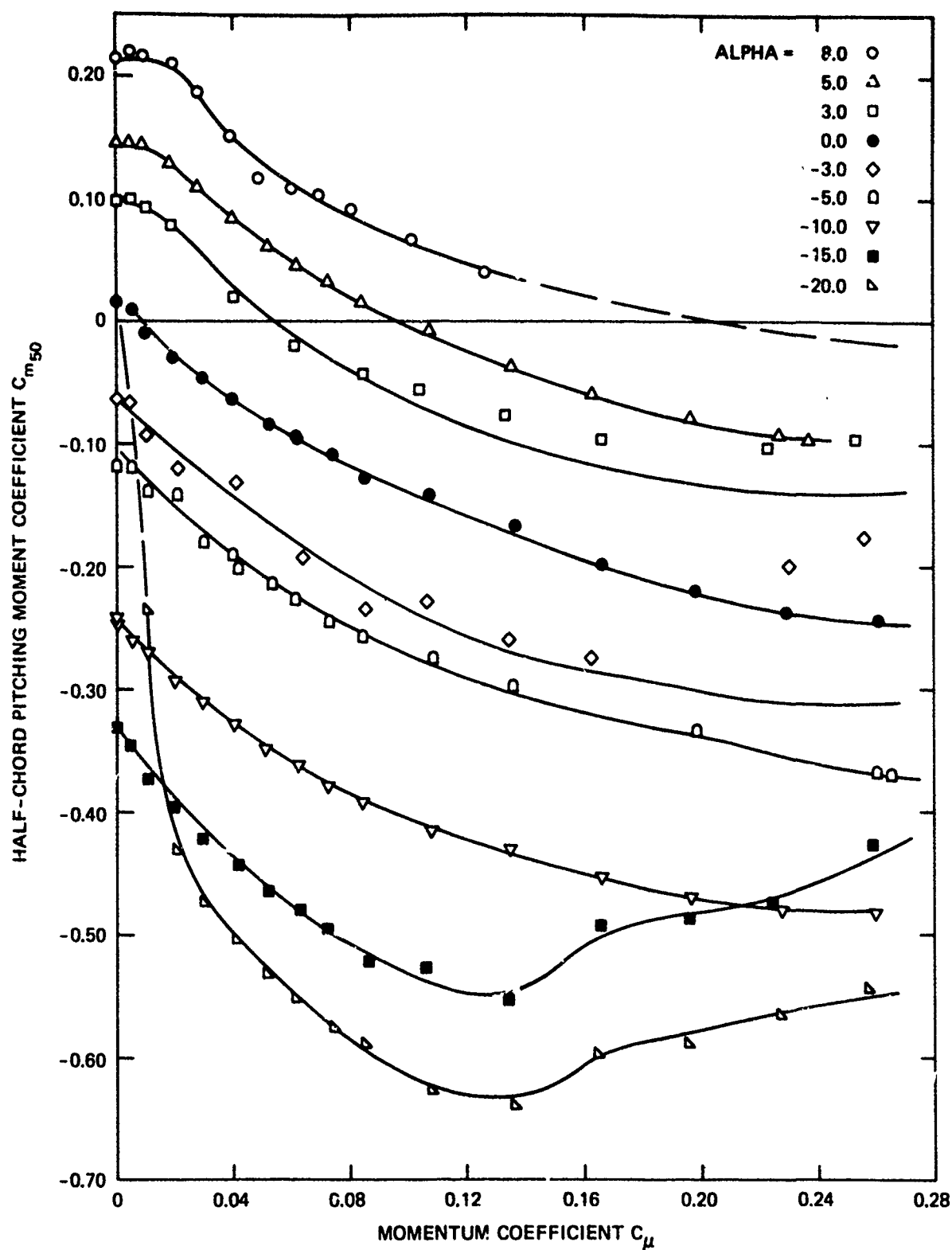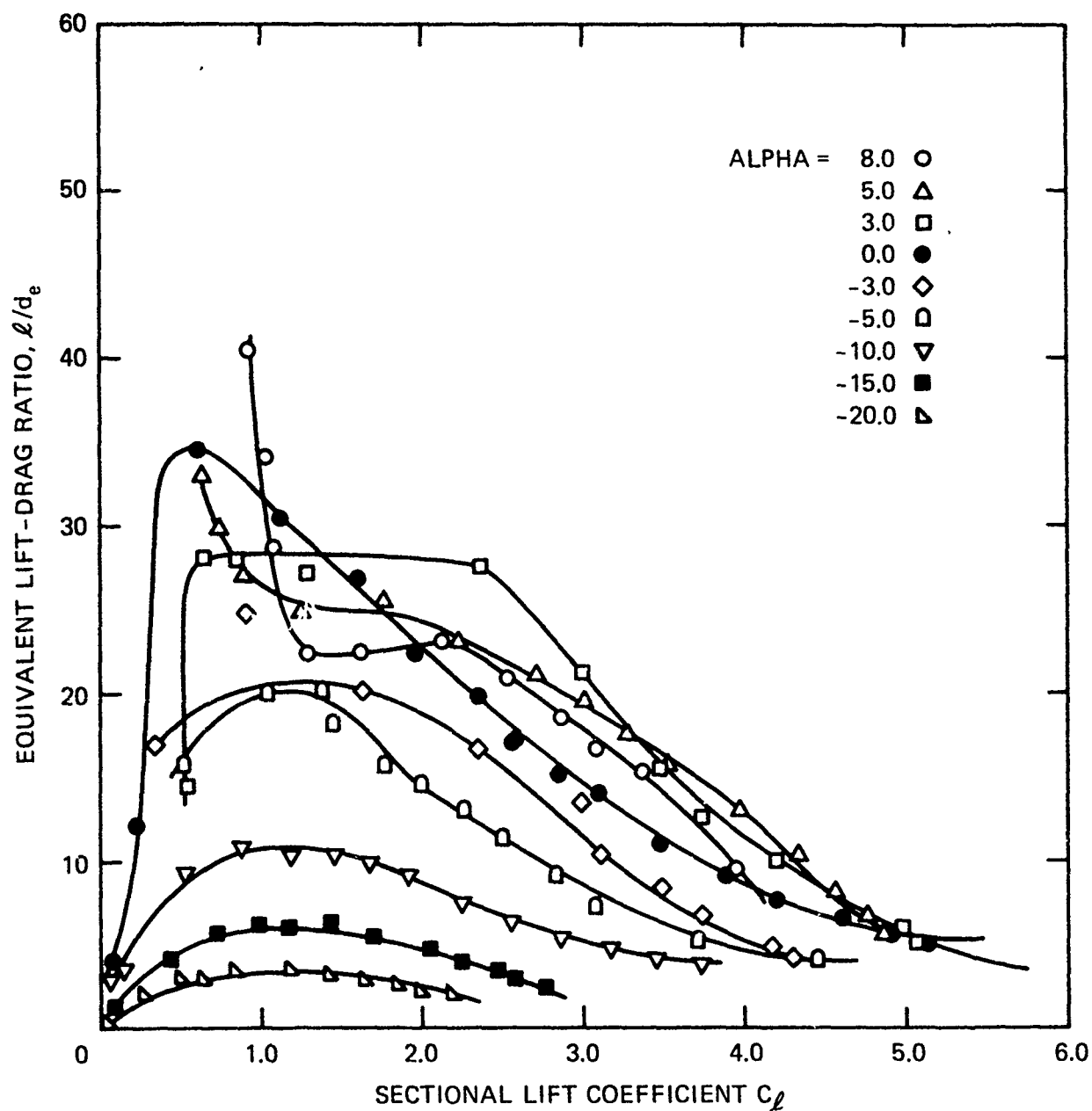
Figure 16 — Equivalent Lift-Drag Ratio as a Function
of Lift Coefficient

TABLE 1

Two-Dimensional Model Coordinates for Upper and Lower Surfaces

Table 1A — Upper Surface			Table 1B — Lower Surface		
X	Y		X	Y	
0.0000	0.0003	LEADING EDGE	7.8980	-0.0364	TRAILING EDGE
0.0200	0.0682		7.8780	-0.0742	
0.0400	0.1095		7.8580	-0.1010	
0.0600	0.1402		7.8280	-0.1340	
0.0799	0.1648		7.7980	-0.1628	
0.1000	0.1859		7.7680	-0.1861	
0.1300	0.2103		7.7380	-0.2081	
0.1600	0.2288		7.6980	-0.2339	
0.1800	0.2429		7.6580	-0.2569	
0.2200	0.2527		7.6180	-0.2774	
0.2500	0.2838		7.5781	-0.2972	
0.2950	0.2993		7.5380	-0.3152	
0.3400	0.3140		7.4930	-0.3340	
0.3850	0.3288		7.4230	-0.3611	
0.4300	0.3429		7.3630	-0.3819	
0.4750	0.3569		7.3030	-0.4017	
0.5450	0.3784		7.2530	-0.4166	
0.7050	0.4245		7.0930	-0.4595	
0.8650	0.4651		6.9330	-0.4963	
1.0250	0.5010		6.7730	-0.5291	
1.2250	0.5401		6.6130	-0.5584	
1.3850	0.5672		6.4530	-0.5829	
1.6050	0.6008		6.2930	-0.6055	
2.0050	0.6509		5.8779	-0.6551	
2.4050	0.6893		5.3780	-0.7010	
2.8050	0.7181		4.8780	-0.7328	
3.2050	0.7367		4.3780	-0.7499	
3.6300	0.7485		3.8780	-0.7545	
4.1300	0.7522		3.4030	-0.7515	
4.5050	0.7464		3.0030	-0.7403	
5.0051	0.7257		2.6030	-0.7169	
5.5050	0.6930		2.2030	-0.6828	
6.0050	0.6428		1.8030	-0.6363	
6.3350	0.6000		1.4630	-0.5851	
6.4950	0.5771		1.3030	-0.5573	
6.6550	0.5520		1.1430	-0.5279	
6.8150	0.5238		0.9830	-0.4947	
6.9750	0.4922		0.8230	-0.4569	
7.1350	0.4557		0.6630	-0.4130	
7.2700	0.4191		0.5030	-0.3622	
7.3300	0.4011		0.4430	-0.3419	
7.3900	0.3814		0.3830	-0.3208	
7.4500	0.3595		0.3229	-0.2993	
7.5100	0.3357		0.2630	-0.2761	
7.5500	0.3180		0.2180	-0.2565	
7.5900	0.2988		0.1680	-0.2311	
7.6300	0.2779		0.1380	-0.2121	
7.6700	0.2546		0.1080	-0.1898	
7.7100	0.2292		0.0780	-0.1617	
7.7500	0.2015		0.0480	-0.1236	
7.7900	0.1696		0.0280	-0.0883	
7.8201	0.1418		0.0080	-0.0346	LEADING EDGE
7.8500	0.1099				
7.8800	0.0696				
7.9000	0.0281				
7.9080	0.0000	TRAILING EDGE			

TABLE 2
Two-Dimensional Model Pressure Tap Coordinate Listing

Upper Surface		Lower Surface	
Tap No.	X Position	Tap No.	X Position
1	0	55	0.125
2	0.084	54	0.205
3	0.177	53	0.301
4	0.285	52	0.396
5	0.410	51	0.606
6	0.590	50	0.801
7	0.782	49	1.188
8	1.186	48	1.601
9	1.591	47	2.011
10	2.001	46	2.421
11	2.403	45	2.801
12	2.795	44	3.210
13	3.184	43	3.624
14	3.618	42	4.293
15	4.295	41	4.743
16	4.747	40	5.194
17	5.201	39	5.601
18	5.603	38	5.991
19	5.996	37	6.400
20	6.394	36	6.806
21	6.799	35	7.191
22	7.201	34	7.437
23	7.666	33	7.649
24	7.710	32	7.737
25	7.723	31	7.848
26	7.801	30	7.888
27	7.843	29	7.906
28	7.885		
29	7.906		